

白云石与富硅流体的水-岩反应实验及其 储层地质意义

王小林^{1,2}, 万野¹⁾, 胡文瑄^{1,2)}, 尤东华^{1,3)}, 曹剑^{1,2)}, 朱东亚⁴⁾, 李真⁵⁾

1) 南京大学地球科学与工程学院, 中国南京, 210023;

2) 南京大学能源科学研究院, 中国南京, 210023;

3) 中国石化石油勘探开发研究院无锡石油地质研究所, 中国江苏无锡, 214151;

4) 中国石化石油勘探开发研究院, 中国北京, 100083;

5) 科廷大学应用地质学系地球科学研究所, 澳大利亚珀斯, 6485

内容提要:含硅热液是影响深层白云岩储层的一种重要的流体类型,其如何与白云岩相互作用以及能否促使深层有效白云岩储层发育,是当前流体地质学与碳酸盐储层地质学研究需要进一步揭示的科学问题。本文以 $\text{CaMg}(\text{CO}_3)_2\text{-SiO}_2\text{-H}_2\text{O}$ 体系为例,应用熔融毛细硅管合成包裹体技术和原位激光拉曼光谱分析技术,结合淬火微区X衍射、扫描电镜观察及能谱分析等手段,研究了富硅流体与白云石的水岩反应机理。结果表明,白云石与富硅流体在100℃以上即可发生脱碳反应产生 CO_2 ,200℃时的反应机理为: $3\text{CaMg}(\text{CO}_3)_2$ (白云石) + $4\text{SiO}_2 + \text{H}_2\text{O} = \text{Mg}_3(\text{Si}_4\text{O}_{10})(\text{OH})_2$ (滑石) + $3\text{CaCO}_3 + 3\text{CO}_2$ 。据此,认为滑石这类富镁硅酸盐矿物可以作为白云岩储层含硅热流体作用的证据。深部富硅热液沿断裂向上运移,与白云岩反应后沉淀滑石等富镁硅酸盐矿物,继而导致储集空间的减少,但是气相产物 CO_2 是重要的酸性气体,可以在合适的地质条件下溶蚀碳酸盐矿物,有利于深埋条件下储集空间的形成与保存。

关键词:白云石;含硅热液;水岩反应;滑石;碳酸盐储层

热液作为一种重要的地质营力,其对储层,特别是碳酸盐储层形成的作用越来越受到重视。碳酸盐岩层系中热液流体的活动可以导致大规模的热液白云岩化(Qing Hairuo and Mountjoy, 1994; Warren, 2000; Machel, 2004; Davies and Smith, 2006),对于埋藏条件下孔隙的形成和保存具有重要意义(Qing Hairuo and Mountjoy, 1994; Davies and Smith, 2006; Luczaj et al., 2006; Slater and Smith, 2012)。国内学者也开展了卓有成效的研究,在四川盆地(刘树根等, 2008; 舒晓辉等, 2012; 黄思静等, 2014; 唐雪松等, 2016; Feng Mingyou et al., 2017)和塔里木盆地(金之钧等, 2006; 潘文庆等, 2009; 朱东亚等, 2009; 焦存礼等, 2011; Dong Shaofeng et al., 2013; Zhu Dongya et al., 2015a)等含油气盆地的海相碳酸盐岩层系中发现了热液活动的证据,并认为热液溶蚀和热液白云岩化作用对于改善碳酸盐

岩储集物性至关重要。所谓热液, Machel 和 Lonne (2002)建议采用 White (1957)的定义,即不考虑流体成分和来源,只要其温度比围岩高即为热液。基于热液矿物组合、流体包裹体和地球化学分析可以大致描述热液流体的性质和来源(Davies and Smith, 2006)。热液白云岩化流体在成分上肯定是富镁的,其来源具有多样性,如改造的蒸发残余咸水、蒸发岩溶解等(Davies and Smith, 2006)。其他溶蚀性热液流体则含有一定量的酸性组分,按其来源可以分为以下三类:①与岩浆活动有关的热液。例如,塔里木盆地在二叠纪发生了广泛而强烈的岩浆活动,释放出了大量的富氟的热流体。富氟热液沿断裂和裂缝上移,强烈改造奥陶系灰岩,形成了特征的萤石化储层(朱东亚等, 2005, 2008);②与有机质热演化作用有关的热液。沉积有机质在热演化过程中会产生一定量的有机酸和 CO_2 ,这些酸性流

注:本文为国家自然科学基金面上项目(编号:41573054)、重点基金项目(编号:41230312)和中央高校基本科研业务费专项资金项目(编号:020614380056)的成果。

收稿日期:2017-07-03;改回日期:2017-11-01;责任编辑:刘志强。Doi:10.16509/j.georeview.2017.06.017

作者简介:王小林,男,1982年生。博士,副教授,主要从事高温、高压实验和储层地质学等方面的研究。Email: xlinwang@nju.edu.cn。

体进入储层后将碳酸盐等碱性矿物产生一定的溶蚀作用(Seewald, 2003; 兰叶芳等, 2016); ③与硫酸盐热还原作用(TSR)有关的热液。TSR作用将产生酸性气体 CO_2 和 H_2S , 然而其对碳酸盐岩储层孔隙发育的影响尚存争论(Hao Fang et al., 2015; 刘英超等, 2015; 蔡春芳和赵龙, 2016)。

碳酸盐岩层系中的热液流体在很多情况下具有富硅的属性。例如, 除了鞍状白云石外, 石英也是重要的热液充填矿物(刘树根等, 2007; 朱东亚和孟庆强, 2010; Dong Shaofeng et al., 2013; Liu Hong et al., 2016)。然而, 关于硅质热液作用机制的研究却相对薄弱。实际上, 越来越多的勘探实例揭示, 含硅热液对储层的形成有重要影响。例如, 北美大不列颠哥伦比亚的Parkland气田主要产气层位也是硅质岩(Packard et al., 2001); 我国在塔里木盆地顺南地区奥陶系鹰山组灰岩层系(云露和曹自成, 2014; 李映涛等, 2015; 漆立新, 2016)和四川盆地东部二叠系茅口组白云岩层系(唐雪松等, 2016)中发现了与含硅热流体作用有关的优质储层。以塔里木盆地顺南地区鹰山组为例, 含硅热流体作用导致了灰岩的溶蚀和石英的沉淀, 形成了大量的石英晶间孔隙, 硅化层段是天然气的主要产出部位(李映涛等, 2015)。目前研究认为, 含硅热流体沿着深大断裂从深部运移到鹰山组灰岩段, 而鹰山组以下的地层岩性主要为白云岩(Wang Xiaolin et al., 2011a), 含硅热流体对白云岩将会发生怎样的改造作用, 是否如同四川盆地东部二叠系茅口组白云岩层系那样, 主要体现为硅质充填(唐雪松等, 2016), 还需展开系统的深入探讨。

熔融毛细硅管合成包裹体技术是一种近年来兴起的新的人工合成包裹体技术(Chou et al., 2008)。应用该技术可以在室温条件下方便地合成各种有机、无机包裹体(Chou et al., 2008; Pan Zhiyan et al., 2009; Wang Xiaolin et al., 2011b, 2013a; Yuan Shunda et al., 2013)。这种微小的(长约2 cm, 内径约50~500 μm)熔融硅管胶囊也可以作为高温高压实验的反应腔(Pan Zhiyan et al., 2009; Yuan Shunda et al., 2013)。由于腔体透明, 除了常规的淬火分析外, 还可以利用显微镜和光谱仪对反应过程进行实时监控。此外, 熔融毛细硅管的成分为 SiO_2 , 在进行含硅流体参与的高温高压实验时, 不需要额外引入 SiO_2 。因此, 引入熔融毛细硅管合成包裹体技术可为研究含硅热液作用下的储层发育机制提供解决途径。本文应用熔融毛细硅管合成包裹

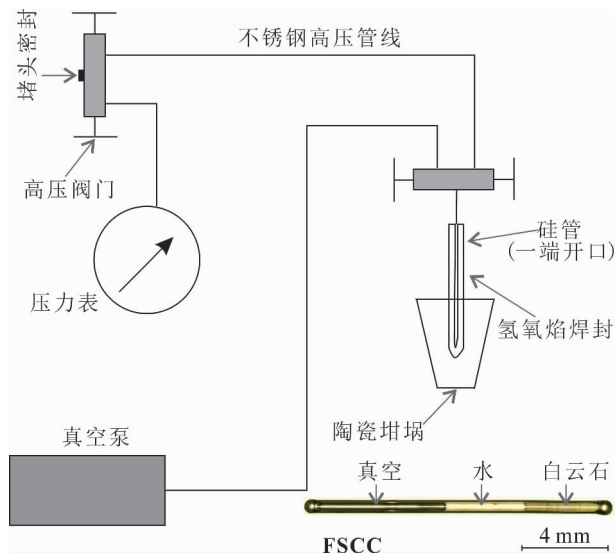


图1 熔融毛细硅管胶囊装样系统示意图和制备好的样品
Fig. 1 A schematic figure showing the FSCC loading system, and a prepared FSCC containing dolomite and water

体技术, 结合原位拉曼光谱和淬火微区X-衍射、扫描电镜、能谱分析等多种分析手段, 开展了 $\text{CaMg}(\text{CO}_3)_2$ (白云石)— SiO_2 — H_2O 体系在储层温度条件下(60~200 $^{\circ}\text{C}$)的水岩反应实验, 进一步结合已有地质实例, 探讨了含硅热液对碳酸盐岩储层的影响, 并讨论了今后实验研究应关注的问题。

1 实验方法

1.1 样品制备

白云岩样品产自四川盆地灯影组, 粉末X衍射分析结果显示, 其矿物组成主要为白云石(>97%)和石英(<3%)。水为电阻率大于18.2 $\text{k}\Omega$ 的去离子水。反应腔为熔融毛细硅管胶囊(Fused silica capillary capsule, FSCC)(Chou et al., 2008), 其组分为熔融 SiO_2 , 因此不需要额外提供 SiO_2 作为反应物。关于FSCC的制备方法, Chou等(2008)已做过详细描述。本次实验所用的熔融毛细硅管横截面为圆形, 其外径和内径分别为0.65 mm和0.50 mm。首先, 截取长约6 cm的熔融毛细硅管, 将其表面的聚酰亚胺保护层烧掉, 并利用氢氧焰将其一端焊封。然后, 将白云石粉末和长约0.5 cm的水柱装入硅管, 并离心至焊封端。这时, 将硅管的开口端接至压力管线并抽真空, 最后利用氢氧焰焊封开口端(图1)。在抽真空和焊封阶段, 含样品的硅管部分一般浸入冷水或液氮中。制备好的FSCC长约2 cm, 其中固相组分和水的长度均为0.5 cm, 真空段

长约 1 cm (图 1)。为了对比分析,也制备了部分含方解石粉末和水的 FSCC 样品。

1.2 原位观测

含硅热流体如果与白云石发生脱碳反应,其气相产物必然含有 CO_2 ,而拉曼光谱可以检测到微量的 CO_2 (Rosso and Bondar, 1995)。例如,已有研究表明,拉曼光谱可以检测到室温条件低至 0.05 ~ 0.06 MPa 的 CO_2 (Rosso and Bondar, 1995; Lamadrid, 2016)。因此,气相组分中是否有 CO_2 可做作为水岩反应是否发生的指示。本次实验使用 Linkam CAP500 型热台控制样品的反应温度,其控温精度为 $\pm 0.1^\circ\text{C}$ 。实验前,应用 K 型热电偶对该热台进行温度校正。结果表明,在 300°C 时,热台中部 4 cm 的范围内温差小于 0.5°C ,表明热台温度分布均匀。拉曼光谱仪型号为 LabRAM HR800, Horiba JY, 激发波长为 532.11 nm, 配备 50 倍长工作距离物镜及 1800 刻线/毫米光栅,对应的光谱分辨率优于 1 cm^{-1} 。收集光谱前,利用 Si 的 520.2 cm^{-1} 峰对拉曼光谱仪进行校正 (Parker et al., 1967)。气相组积分时间为 120 s, 固相组积分时间为 30 s。所采集光谱应用 Labspec 5 软件进行分析以获得峰强、峰位等信息。首先将 FSCC 加热至 60°C , 加热约 24 h 后原位采集反应腔中气相组分的拉曼光谱,若未检测到 CO_2 信号,升高 10°C 继续重复上述程序,直至确认气相组分中含有 CO_2 。此外,为了分析反应速率和检验反应是否达到平衡,将一 FSCC 置于热台内加热至 200°C 反应约 10 d, 收集不同反应时间 FSCC 中气相 CO_2 信号,并对比 CO_2 信号强度随反应时间的变化规律。

1.3 淬火分析

将含有去离子水和白云石粉末的一端开口的熔融毛细硅管置于内衬有聚四氟乙烯 (PTFE) 的不锈钢反应釜 (10 ml) 中加热。考虑到低温时反应速率较慢,且固体产物较少,因此设定反应温度为 $150\sim 200^\circ\text{C}$, 反应时间为 20 ~ 80 d。加热过程中,多次打开反应釜以释放产生 CO_2 , 从而获得一定量的固体产物,便于拉曼光谱、微区 X 衍射和扫描电镜分析。微区 X 衍射仪型号为 Rigaku D/max Rapid II, 装备钨靶, 准直管的半径为 0.3 mm, 样品台转动的角速度为 $6^\circ/\text{s}$, 仪器的工作电流为 90 mA, 加速电压为 50 kV, 扫描时长为 10 ~ 20 min。利用 Jade 6.0 软件对获得的 X 衍射图谱进行分析。拉曼光谱和微区 X 衍射分析完成以后,打破硅管,取出固体样品,应用蔡司 Supra55 场发射扫描电镜观察反应

后固相矿物的形貌,并结合能谱仪 (EDX, Oxford Instruments, Inca X-Max 150 mm^2) 半定量分析固相的化学成分。

2 实验结果

2.1 气相组分

如前所述,含硅热流体如果与白云石发生水岩反应,其气相产物必然含有 CO_2 。 CO_2 的拉曼光谱以位于 1280 cm^{-1} 和 1380 cm^{-1} 附近的费米峰为特征 (Wright and Wang, 1973; Rosso and Bodnar, 1995; Dubessy et al., 1999), 其拉曼位移和峰间距是定性和定量分析流体包裹体中 CO_2 组分的重要指标 (Rosso and Bodnar, 1995; Song Yucai et al., 2009; Wang Xiaolin et al., 2011b; Frezzotti et al., 2012)。如图 2a 所示,本次实验加热至 100°C 持续反应 24 h 后,可以在气相组分中检测到 CO_2 的费米峰;而当加热到 200°C 时,反应 2 h 后气相组分中 CO_2 的信号已经比较明显,并且随着反应时间的延长, CO_2 信号逐渐增强。相比而言,含方解石和水的 FSCC 样品即使加热到 150°C , 在气相中也检测不到 CO_2 信号。

此外,当反应时间相同时,温度越高,气相组分中 CO_2 的信号越强。例如,加热 24 h 后,反应温度为 200°C 的 FSCC 中 CO_2 的浓度要明显高于反应温度为 100°C 的样品 (图 2a)。图 2b 是反应温度为 200°C 时, CO_2 费米高频峰面积、低频峰面积以及高频峰和低频峰总面积随反应时间的变化规律。在一定的实验条件下,拉曼活性组分的峰面积 (或峰强) 与其单位体积内的分子数呈正比。当反应时间小于 40 h 时, CO_2 峰面积随着反应时间的增加快速增长;反应时间在 40 ~ 120 h 之间时, CO_2 峰面积随时间延长缓慢增加;当反应时间超过 120 h 之后, CO_2 峰面积基本保持不变。

在一定的温度条件下, CO_2 费米峰间距随着 CO_2 密度 (压力) 的增大而增加 (Garrabos et al., 1980)。因此,可以根据 CO_2 费米峰峰间距获得 CO_2 的密度或者压力,前人据此建立了多个 CO_2 费米峰间距和密度关系的方程式 (Rosso and Bodnar, 1995; Yamamoto and Kagi, 2006; Song Yucai et al., 2009; Fall et al., 2011; Wang Xiaolin et al., 2011b; 陈勇, 2015; Lamadrid, 2016)。用于建立上述方程式的 CO_2 压力低至 0.06 MPa。然而,我们在应用费米峰间距计算 CO_2 产物的压力时,得出的结果为负值。

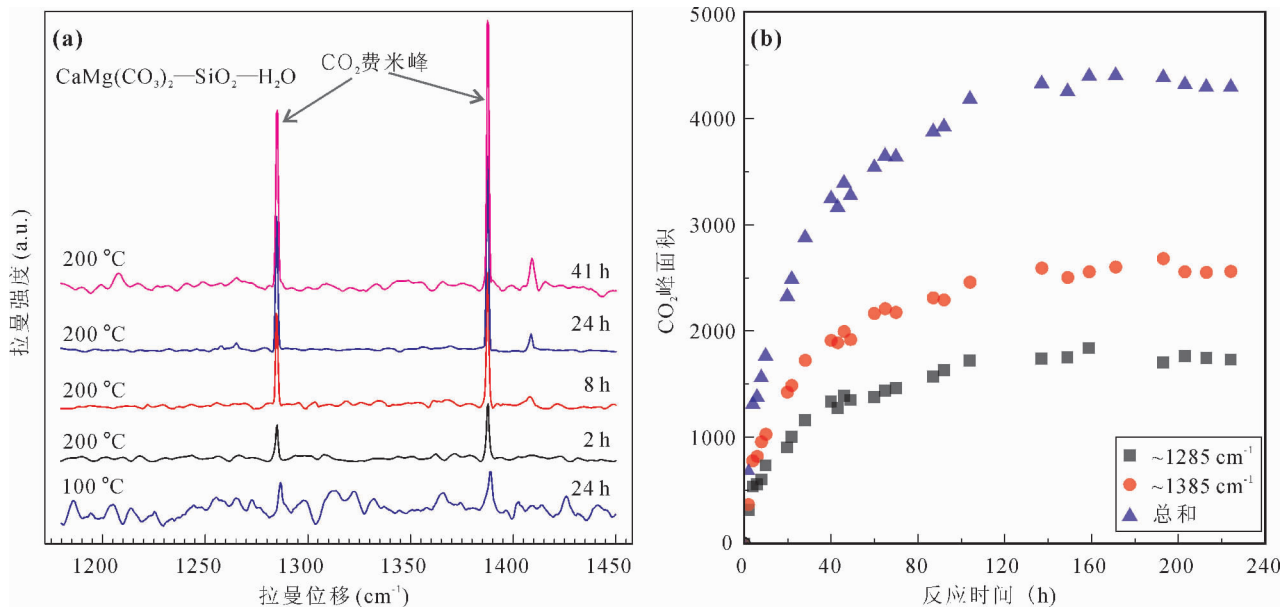


图2 (a) 典型样品气相产物拉曼光谱; (b) CO₂ 费米峰面积随反应时间变化规律(200°C)

Fig. 2 (a) In situ Raman spectra of the vapor phases of two FSCCs containing dolomite and water; (b) variations in the peak areas of the CO₂ Fermi bands with experimental duration (200°C). Square and circle represent the peak areas of the lower band and the upper band, respectively. Triangle is the peak area of the total Fermi bands

2.2 固相组分

通过拉曼光谱分析, 查明了含硅热流体与白云石水岩反应的产物。如图3a, 反应前固相拉曼光谱中仅能识别出白云石的特征峰 (~177, 300.5, 1098 cm⁻¹; Nicola et al., 1976), 这与X衍射分析

结果一致, 说明白云石纯度较高。加热至200°C并恒温60 d后, 在固相产物的拉曼光谱中还检测到了滑石(190.5, 360.5, 675 cm⁻¹; Rosasco and Blaha, 1980)和方解石(282, 1086 cm⁻¹; Gunasekaran et al., 2006)的特征峰。可见, 白云石和含硅热流体

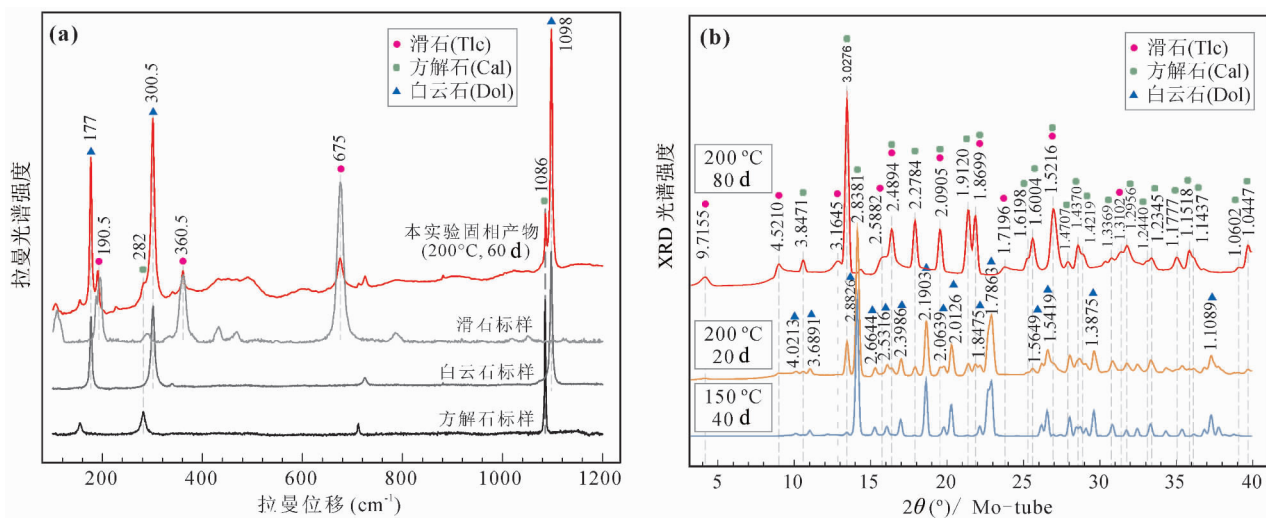


图3 (a) 固相产物拉曼光谱分析结果; (b) 固相产物微区X衍射分析结果

Fig. 3 (a) Raman spectrum of the solid phase in an FSCC containing dolomite and water after heating at 200°C for 60 days. Raman spectra of calcite, dolomite and talc were also presented for reference; (b) micro-X-ray diffraction patterns of the solid phase in FSCCs containing dolomite and water after heating at 150°C for 40 days and at 200°C for 20 days and 80 days. Cal, Dol and Tlc represent calcite, dolomite and talc, respectively

水岩反应的固相产物是滑石和方解石。

为了进一步确认固相产物的矿物组成,开展了系统的微区 X 衍射分析。如图 3b, 在 200℃ 反应 20 d 后, 残余固相中矿物组成主要为白云石, 此外, 也检测到少量的方解石和滑石的信号。继续加热 60 d 后, 固相矿物组成主要为方解石和滑石, 而白云石的信号几乎不可见。然而, 加热至 150℃ 并恒温 40 d 后, 残余固相的矿物组分主要为白云石和少量方解石, 没有检测到滑石或其他镁硅酸盐矿物的特征峰。

图 4 是反应后固相组分的扫描电镜观测和能谱分析结果, 反应条件为 200℃, 60 d。滑石呈片状, 局部包裹白云石晶体, 在白云石晶体表面观察到大量纳米自形方解石(图 4a, b)。白云石溶蚀现象明显(图 4c), 甚至能够观察到白云石溶蚀的阶梯状残余晶体(图 4d)。白云石粉末被封入硅管后, 与内管壁接触的部分反应最为强烈, 可以观察到绕硅管内壁分布的包壳状滑石(图 4d, 箭头)。但是, 固相组分内部仍然形成了大量滑石, 其产状与包壳状滑石截然不同, 主要呈片状分布于白云石周围(图 4a, c~e)。此外, 图 4e 中典型测点的能谱分析结果进一步证实了固相产物是滑石和方解石。

3 讨论

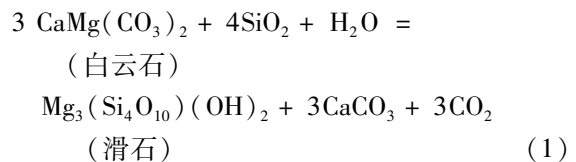
3.1 含硅热流体对碳酸盐储层发育的影响

3.1.1 含硅流体参与下的白云石脱碳反应

前人研究指出, 白云石与 SiO_2 相互作用形成滑石是 $\text{CaO—MgO—SiO}_2\text{—H}_2\text{O—CO}_2$ 体系 (CMSC) 最初级的变质作用 (Holness, 1997)。根据理论计算结果, 白云石与含硅流体在 150℃ 即可反应形成滑石 (李明德, 1991; Holness, 1997; Tornos and Spiro, 2000)。然而, 地质研究表明, 白云石发生滑石化所需温度较高, 一般在 250 到 400℃ 之间 (Hecht et al., 1999; 陈从喜等, 2003; Boulvais et al., 2006; Sharma et al., 2009)。也有学者开展了相关的高温高压模拟实验, 但是反应温度一般均高于 250℃ (Gordon and Greenwood, 1970; Bayliss and Levinson, 1971; Skippen, 1974; Slaughter, 1975; Eggert and Kerrick, 1981), 这样的实验温度高于绝大多数含油气盆地白云岩层系的热液作用温度 (如 Davies and Smith, 2006)。

本项实验结果显示, 白云石与含硅流体在 100℃ 即可反应形成 CO_2 。在本实验的温度范围内, 相同的温度条件下方解石的溶解度高于白云石

(Shock and Helgeson, 1988; Pokrovsky et al., 2009)。前人研究表明, 白云石热分解产生 CO_2 需要更高的温度条件 (662℃, 陈永弟, 2012; > 500℃, 蒋晓光等, 2012)。因此, 含白云石的 FSCC 气相产物中的 CO_2 不可能来自白云石的溶解和白云石的热分解, 而是通过脱碳化反应形成的, 进一步说明白云石在 100 ~ 200℃ 条件下即可与含硅流体相互作用形成 CO_2 和镁硅酸盐。受到固相产物量的制约, 我们只确认了 200℃ 时固相产物的组分, 认为白云石和含硅流体在 200℃ 发生如下反应:



也就是说, 白云石与含硅流体在 200℃ 即可反应形成滑石、方解石和 CO_2 ; 在 100 ~ 200℃ 之间, 白云石在含硅流体中也会发生脱碳反应形成 CO_2 , 结合前人理论计算结果, 形成的富镁硅酸盐很可能也是滑石 (李明德, 1991; Holness, 1997; Wan Ye et al., 2017)。从图 4d 可以看出, 滑石除了沿硅管内壁分布以外, 也出现在固相组分的内部, 表明部分溶解态的 SiO_2 与白云石反应形成滑石、方解石和 CO_2 , 也支持文中的“白云石与含硅流体反应”这一说法。

气相产物 CO_2 费米峰面积随反应时间的变化规律可以用来探讨该反应的动力学特征。如实验结果部分所述, 在 200℃ 时, 白云石与含硅流体之间的反应速率在 40 h 以内时较高, 之后反应速率放缓, 到 120 h 以后基本达到平衡。200℃ 实验条件下, 应用平衡后 CO_2 费米峰间距计算得到的 CO_2 密度为负数, 说明 CO_2 分压在室温条件下小于 0.06 MPa (Lamadrid, 2016)。因此, 尽管白云石和 SiO_2 在 100 ~ 200℃ 条件下即可反应形成 CO_2 及镁硅酸盐, 但是在封闭体系下形成的 CO_2 量有限。此外, 反应速率受温度控制明显, 即反应速率随温度升高而加快, 证据有二: ① 相同反应时间内 (24 h), 200℃ 条件下气相产物 CO_2 的信号强于 100℃; ② 在 200℃ 条件下, 反应 20 d 即可检测到滑石和方解石等固相产物, 而在 150℃ 条件下, 反应 40 d 依然检测不到滑石的信号。

3.1.2 滑石指示含 Si 流体作用

近年来, 学者在硅化强烈的碳酸盐储层中发现了滑石等富镁硅酸盐矿物。例如, 唐雪松等 (2016) 研究了四川盆地东部中二叠统茅口组储层的成岩作

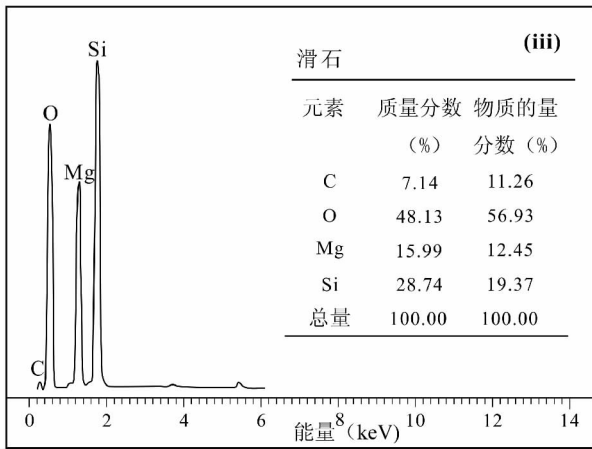
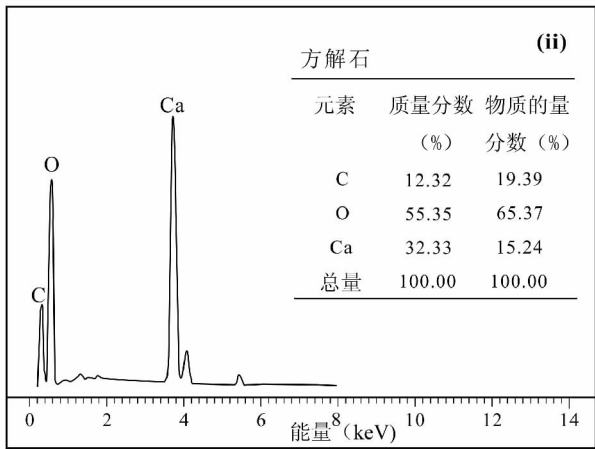
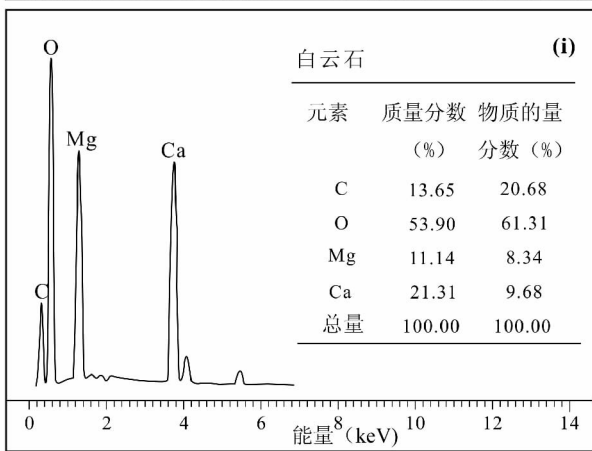
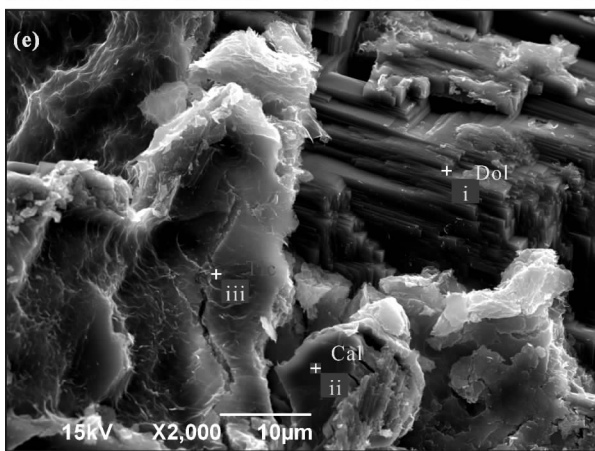
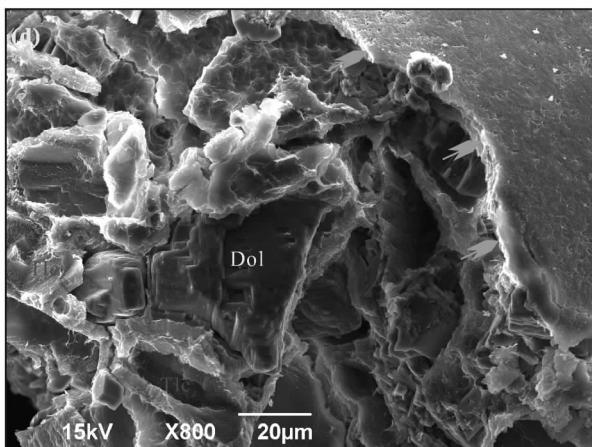
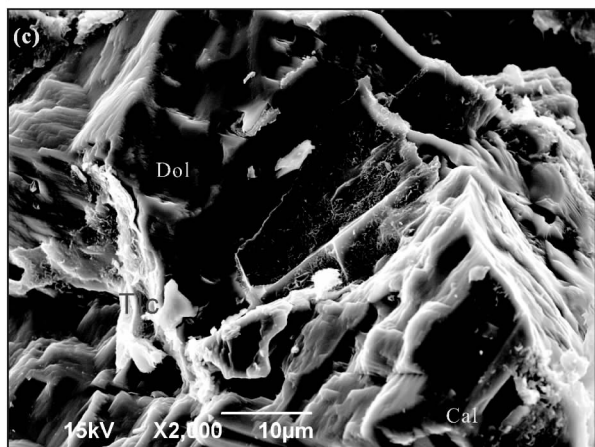
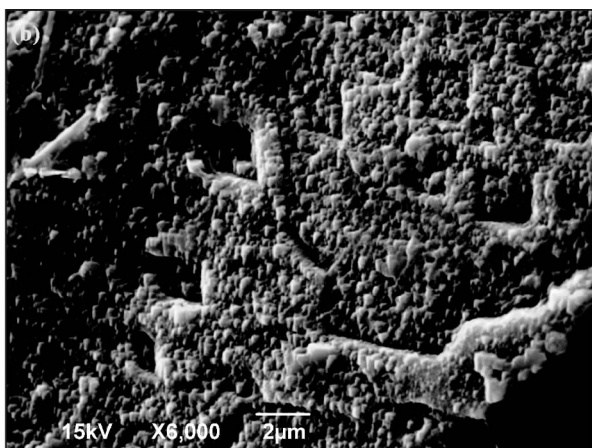
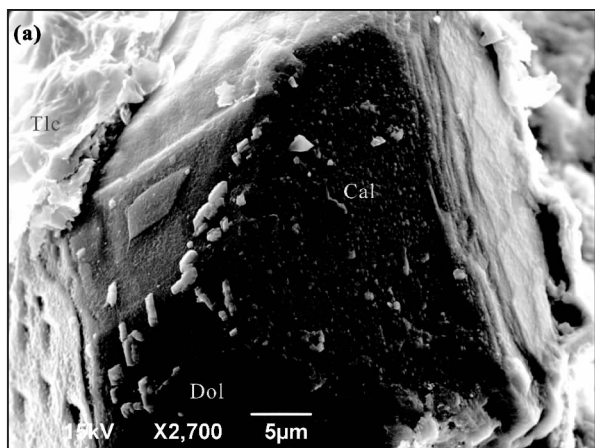


图 4 固相产物扫描电镜观测和能谱分析结果(反应条件为 200℃, 60 d)

Fig. 4 Field emission scanning electron microscope (FE-SEM) observations and energy dispersive spectrometer (EDS) analyses of the solid phase in an FSCC containing dolomite and water after heating at 200℃ for 60 days

(a) 片状滑石覆盖在白云石晶体上, 白云石表面分布大量纳米自形方解石; (b) 纳米自形方解石; (c) 片状滑石, 白云石溶蚀强烈, 晶面凹凸不平, 而方解石晶形较好; (d) 与硅管内壁接触的滑石包壳(箭头), 阶梯状溶蚀残余白云石和其周边的滑石; (e) 典型能谱分析测点位置及能谱分析结果。Cal、Dol 和 Tlc 分别代表方解石、白云石和滑石

(a) Dolomite was surrounded by sheet-like talc minerals. Plenty of nano-scale euhedral calcites were also observed on the dolomite surface; (b) magnification of (a) showing newly formed nano-scale euhedral calcites; (c) sheet-like talc and subhedral calcite. Dolomite experienced strong erosion and has uneven crystal faces; (d) cylindrical talc on the inner surface of the fused silica capillary tube (arrow). Residual dolomite showed a ladder-like structure and was surrounded by talc; (e) typical EDS analyzing positions, and the EDS analyses of dolomite (i), calcite (ii) and talc (iii). Cal, Dol and Tlc represent calcite, dolomite and talc, respectively

用, 认为热液白云岩化和含硅热流体活动主要沿早期岩溶系统发育, 含硅热流体交代白云岩, 形成了特殊的硅质白云岩和白云质硅岩储层。然而, 含硅热液对储层的改造主要体现在充填孔隙方面, 降低了储层的孔隙度和渗透性。实际上, 随后的岩心观察表明, 川西北茅口组岩溶系统中充填部分淡绿色滑石。Qing Hairuo (2017) 在分析巴西早白垩世深水碳酸盐储层成岩作用时发现了广泛的硅化作用, 并在薄片尺度上观察到共生的白云石、方解石和滑石。结合我们的实验结果, 可以推测白云岩储层中含硅热流体活动很可能会形成滑石等富镁硅酸盐矿物, 滑石可以作为白云岩储层中含硅流体作用的指示矿物, 其产出和分布具有示踪含硅流体运移路径与作用范围的潜力。

尽管含硅热流体在碳酸盐岩储层中的作用痕迹较为普遍 (Davies and Smith, 2006; Lonnee and Machel, 2006; Luczaj, 2006; Smith, 2006; 刘树根等, 2007; 朱东亚等, 2010; Dong Shaofeng et al., 2013), 却很少有伴生滑石等富镁硅酸盐矿物的相关报道。原因可能有二: ① 如前所述, CO_2 的存在会抑制滑石形成 (Povoden et al., 2002)。 CO_2 是含油气盆地中常见的酸性气体, 有机质热成熟和硫酸盐热还原过程中均会产生大量的 CO_2 (Seewald, 2003; Hao Fang et al., 2015); ② 除了 Mg^{2+} 以外, Al^{3+} 、 K^+ 也是盆地流体重要组分, 而这些离子的存在会促进蒙脱石及其他黏土矿物的形成 (Bayliss and Levinson, 1971)。总之, 含硅热液与碳酸盐岩作用机理除了受岩性、温度、压力控制以外, 还受到流体组分的制约。本实验以 $\text{CaMg}(\text{CO}_3)_2$ - SiO_2 - H_2O 体系为例, 初步探讨了白云石和含硅热流体的作用机制、过程和温度条件。今后需综合考虑岩性、压力和流体组成等变量, 开展系统的高温、高压模拟实验研究, 进一步揭示储层条件下含硅热液与碳

酸盐岩的作用机理。

3.1.3 含硅流体作用对碳酸盐岩储层的影响

最近的地质研究表明, 含硅热流体与碳酸盐岩作用不会形成富镁硅酸盐矿物, 而是以溶蚀灰岩和沉淀(微晶)石英为主。例如, 在塔里木盆地顺南地区奥陶系鹰山组灰岩地层, 含硅热流体作用形成了特殊的硅质岩优质储层(云露和曹自成, 2014; 李映涛等, 2015; 漆立新, 2016)。流体包裹体测温结果显示, 石英中原生流体包裹体的均一温度在 201~252℃ 之间(李映涛等, 2015)。漆立新(2016)认为含硅热液来自深部地层, 沿深大断裂运移到上部鹰山组, 溶蚀灰岩并沉淀石英。鹰山组以下奥陶系和寒武系地层主要岩性是白云岩, 在如此高的温度条件下, 含硅热液在其运移通道周围很可能与白云石反应形成滑石等富镁硅酸盐矿物。除了充填孔隙外, 白云石脱碳作用还会产生酸性气体 CO_2 , 其沿深大断裂上移, 在浅部也会造成碳酸盐的溶蚀 (Giles and Marshall, 1986; Pokrovsky et al., 2005; Duan Zhenhao and Li Dedong, 2008; Pokrovsky et al., 2009)。例如, 鹰山组硅质岩层段石英包裹体中检测到的 CO_2 (李映涛等, 2015) 可能也有深部白云石脱碳作用的贡献。根据反应式(1), 当富硅流体作用于灰岩地层时, 适量 CO_2 的存在将利于白云石的产生, 而硅质岩层段缺少白云石也表明含硅热液贫镁(李映涛等, 2015)。加拿大不列颠哥伦比亚省 Parkland 气田的主要储层也是硅质岩, 主要由大量微晶石英组成 (Packard et al., 2001)。硅质岩储层位于上泥盆统 Wabamun 群顶部灰岩和白云岩的过渡层段。流体包裹体测温结果表明, 含硅热液的作用温度为 140~200℃ 之间。然而, 在如此高的温度条件下, Packard 等(2001)并没有观察到含硅热液交代白云石形成滑石等富镁硅酸盐矿物的现象, 相反地, 含硅热液选择性交代灰岩, 而对前期形成

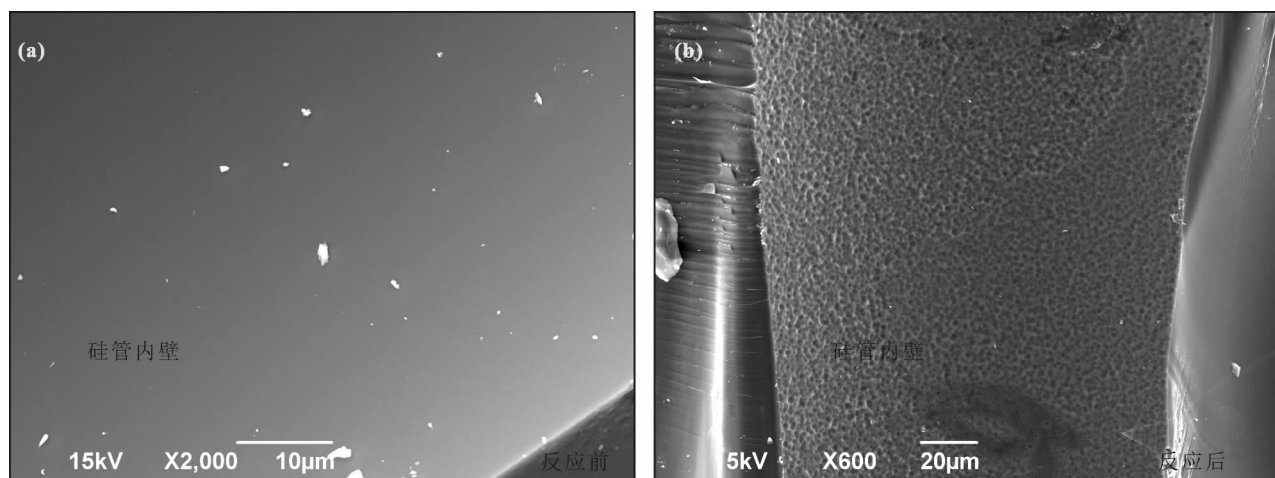


图5 反应前后硅管内壁扫描电镜照片

Fig. 5 SEM images of the inner surface of an FSCC containing dolomite and water before and after heating

(a) 反应前硅管内壁光滑; (a) 反应后(200 °C, 60 d) 硅管内壁布满溶蚀坑

(a) Smooth inner surface before heating; (b) the inner surface is full of etch pits after heating at 200 °C for 60 days

的白云石没有明显的改造作用。他们将该现象解释为含硅热液对白云石饱和,而对灰岩不饱和。该气田产出的天然气中含5%~7%的CO₂,如果其聚集先于含硅热液侵入或与含硅热液作用同时,那么抑制滑石形成的因素可能也是较高的CO₂含量(Povoden et al., 2002)。此外,这也解释了为何发生溶蚀的是灰岩,而不是白云石(反应式1)。

白云石与含硅流体作用是否创造储集空间受控于硅的来源。如果热液流体仅创造高温环境,而硅来自于白云岩储层中的石英等,则该反应将创造额外的孔隙:McKinley等(2001)的研究显示,白云石与石英相互作用形成滑石、方解石和CO₂将使矿物总体积减少13%~17%。而当热液本身含硅,则该反应将导致矿物总体积增大,破坏原有的储集空间。以林传仙等(1985)发表的298.15 K时矿物摩尔体积数据计算,当白云石(64.34 ± 0.03 cm³/mol)与含硅热液反应形成滑石(136.25 ± 0.26 cm³/mol)和方解石(64.34 ± 0.015 cm³/mol)时,矿物总摩尔体积将增大27.95%。然而,该反应产生的CO₂是重要的酸性气体,可能是碳酸盐岩层系中CO₂的重要来源之一,对于深埋条件下孔隙的发育和保存具有重要意义(Zhu Dongya et al., 2015b)。

3.2 对硅管实验的启示

熔融毛细硅管具有良好的耐热、耐高压、耐腐蚀和透光性强等优点,可以作为人工合成包裹体和高温高压实验的腔体(Chou et al., 2005, 2008)。结合拉曼光谱等分析手段,能够开展拉曼光谱定量分

析流体包裹体组分(Lu Wanjun et al., 2007; Wang Xiaolin et al., 2011b, 2013b)、气体在溶液和熔融硅中的扩散系数(Shang Linbo et al., 2009; Lu Wanjun et al., 2013)、流体中元素的赋存方式和离子络合作用(Dargent et al., 2013; Wang Xiaolin et al., 2013a, 2016a, b, c, 2017; Wan Ye et al., 2015)、硫酸盐还原反应机理(Yuan Shunda et al., 2013)以及有机质降解(Pan Zhiyan et al., 2009)等研究。应用熔融毛细硅管制备的光学腔体,其可承受的温度、压力受硅管规格控制(内外径尺寸等),最高可达650 °C和300 MPa。

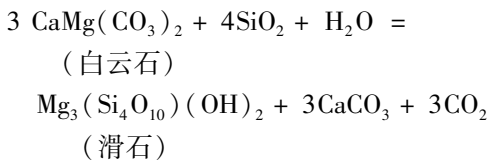
在本次实验中,硅管(SiO₂)作为反应物与白云石和水反应形成滑石(反应1),对硅管内壁造成了强烈腐蚀。如图5所示,反应前硅管内壁光滑,而反应后则布满了溶蚀坑,必然会降低硅管的机械强度。此外,SiO₂的溶解度随着温度升高而增大,在碱性溶液中溶解度更高(Fleming and Crerar, 1982)。例如,在中性溶液中,SiO₂在20 °C时溶解度为100 × 10⁻⁶,而当温度升至310 °C后,其溶解度增加至1500 × 10⁻⁶(Marshall, 1980; Chen and Marshall, 1982; Gunnarsson and Arnórsson, 2000)。因此,在应用熔融毛细硅管作为反应腔开展高温高压实验时,应考虑SiO₂的溶解度和反应活性,SiO₂强烈溶蚀会减弱硅管的机械强度,甚至导致高压反应腔体爆裂和流体泄露。比如,我们在研究Na₂WO₄-H₂O体系的高温相行为时,由于WO₄²⁻的高温水解使得体系呈弱碱性,硅管内壁在350 °C以上

溶蚀明显,如果体系内压较高,在如此高温条件下硅管会发生爆裂。显然, SiO₂的溶蚀也会使得实验体系复杂化,影响实验数据的解释。

4 结论

本文应用熔融毛细硅管作为反应腔,综合原位激光拉曼光谱和淬火微区 X 衍射、扫描电镜观测和能谱分析等技术手段,研究了 CaMg(CO₃)₂—SiO₂—H₂O 体系的水岩反应机理和温度条件,并探讨了其对碳酸盐岩储层发育和应用硅管作为反应腔的高温高压实验研究的启示。主要认识如下:

(1) 白云石与含硅流体在 100℃ 以上即可发生脱碳反应产生 CO₂, 升高温度有利于该反应的进行。根据 200℃ 时反应气相和固相产物的拉曼光谱、微区 X 衍射、扫描电镜观测和能谱分析结果,确定了该反应机理:



从实验的角度证实了白云石与含硅流体在 200℃ 以下即可反应形成滑石(或其他富镁硅酸盐矿物)。反应速率受温度和 CO₂ 含量控制明显,高温和低 CO₂ 含量有利于反应的快速进行;

(2) 白云岩储层中,含硅热液的活动会导致滑石等富镁硅酸盐矿物和 CO₂ 的形成,这些富镁硅酸盐矿物可以作为含硅热流体作用的证据。以塔里木盆地顺南地区为例,深大断裂是含硅热液向上运移的通道,在深部断裂带附近很可能发育含硅热液与白云岩的反应产物,滑石。如果热液仅提供高温反应条件,硅来自储层的石英,则该反应将改善储集空间;如果硅来自热液本身,则该反应将减少原有储集空间。但是气相产物 CO₂ 是重要的酸性气体,在合适的地质条件下可以导致碳酸盐矿物溶蚀,有利于深层碳酸盐岩储层孔隙的发育和保存;

(3) 作为重要的高温高压反应腔,熔融毛细硅管实验技术得到越来越多的研究人员的关注。在实验中,需考虑熔融硅的溶解度和反应活性,因为硅管的溶蚀一方面降低硅管的机械强度,会导致潜在的爆裂和流体泄露的危险;另一方面,熔融硅的溶解会使得研究体系复杂化,影响实验数据的解释。

致谢: 西南石油大学谭秀成教授提供了四川盆地东部茅口组灰岩中热液滑石的基础地质资料。匿名审稿人和编辑认真阅读了文稿并提出了建设性意

见。一并诚致谢忱!

参 考 文 献 / References

(The literature whose publishing year followed by a “&” is in Chinese with English abstract; the literature whose publishing year followed by a “#” is in Chinese without English abstract)

- 蔡春芳, 赵龙. 2016. 热化学硫酸盐还原作用及其对油气与储集层的改造作用: 进展与问题. 矿物岩石地球化学通报, 35(5): 851~859.
- 陈从喜, 倪陪, 蔡克勤, 翟裕生, 邓军. 2003. 辽东古元古代富镁质碳酸盐岩建造菱铁矿滑石矿成矿流体研究. 地质论评, 49(6): 646~651.
- 陈勇. 2015. 流体包裹体激光拉曼光谱分析方法及应用. 东营: 中国石油大学出版社: 20~23.
- 陈永弟. 2012. 白云石的热分解规律及其应用. 导师: 曹占义. 长春市: 吉林大学硕士论文: 1~55.
- 黄思静, 兰叶芳, 黄可可, 吕杰. 2014. 四川盆地西部中二叠统栖霞组晶洞充填物特征与热液活动记录. 岩石学报, 30(3): 687~698.
- 蒋晓光, 王岭, 储刚, 胡晓静, 李卫刚, 刘明杨, 王艳君, 林忠, 盛向军, 陈宇. 2012. X 射线衍射法(XRD)分析煅烧白云石的物相组成. 中国无机分析化学, 2(1): 31~33.
- 焦存礼, 何治亮, 邢秀娟, 卿海若, 何碧竹, 李程成. 2011. 塔里木盆地构造热液白云岩及其储层意义. 岩石学报, 27(1): 277~284.
- 金之钧, 朱东亚, 胡文瑄, 张学丰, 王毅, 闫相宾. 2006. 塔里木盆地热液活动地质地球化学特征及其对储层影响. 地质学报, 80(2): 245~253.
- 李明德. 1991. 白云石蛇纹石化、滑石化的热力学讨论. 矿物岩石, 11(4): 100~104.
- 兰叶芳, 黄思静, 马永坤, 周小康, 卫哲. 2016. 珠江口盆地珠江组碳酸盐岩碳同位素组成负偏的成因意义. 地质论评, 62(4): 915~928.
- 李映涛, 叶宁, 袁晓宇, 黄擎宇, 苏炳睿, 周瑞琦. 2015. 塔里木盆地顺南 4 井中硅化热液的地质与地球化学特征. 石油与天然气地质, 36(6): 934~944.
- 林传仙, 白正华, 张哲儒. 1985. 矿物及有关化合物热力学数据手册. 北京: 科学出版社: 13~30.
- 刘树根, 黄文明, 陈翠华, 张长俊, 李巨初, 戴苏兰, 秦川. 2008. 四川盆地震旦系—古生界热液作用及其成藏成矿效应初探. 矿物岩石, 28(3): 41~50.
- 刘树根, 马永生, 黄文明, 蔡勋育, 张长俊, 王国芝, 盘昌林. 2007. 四川盆地上震旦统灯影组储集层致密化过程研究. 天然气地球科学, 18(4): 485~496.
- 刘英超, 宋玉财, 侯增谦, 杨竹森, 张洪瑞, 马旺. 2015. 伊朗扎格罗斯碰撞造山带马拉耶尔—伊斯拉罕碳酸盐岩容矿铅锌成矿带——矿床基本特征与成因类型. 地质学报, 89(9): 1573~1594.
- 潘文庆, 刘永福, Dickson JAD, 沈安江, 韩杰, 叶瑛, 高宏亮, 关平, 张丽娟, 郑兴平. 2009. 塔里木盆地地下古生界碳酸盐岩热液岩溶的特征及地质模型. 沉积学报, 27(5): 983~994.
- 漆立新. 2016. 塔里木盆地顺托果勒隆起奥陶系碳酸盐岩超深层油气突破及其意义. 中国石油勘探, 21(3): 38~51.
- 舒晓辉, 张军涛, 李国蓉, 龙胜祥, 吴世祥, 李宏涛. 2012. 四川盆地北部栖霞组—茅口组热液白云岩特征与成因. 石油与天然气地质, 33(3): 443~448, 458.
- 唐雪松, 谭秀成, 刘宏, 马腾, 苏成鹏, 程雪莹, 陈虹宇, 曹剑.

2016. 四川盆地东部中二叠统茅口组白云岩及云质硅岩储层特征与发育规律. 石油与天然气地质, 37(5): 731~743.
- 云露, 曹自成. 2014. 塔里木盆地顺南地区奥陶系油气富集与勘探潜力. 石油与天然气地质 35(6): 788~797.
- 朱东亚, 胡文瑄, 宋玉财, 金之钧. 2005. 塔里木盆地塔中45井油藏萤石化特征及其对储层的影响. 岩石矿物学杂志, 24(3): 205~215.
- 朱东亚, 金之钧, 胡文瑄, 张学丰. 2008. 塔里木盆地深部流体对碳酸盐岩储层的影响. 地质论评, 54(3): 348~354.
- 朱东亚, 金之钧, 胡文瑄. 2009. 塔中地区热液改造型白云岩储层. 石油学报, 30(5): 698~704.
- 朱东亚, 孟庆强. 2010. 塔里木盆地地下古生界碳酸盐岩中硅化作用成因. 石油实验地质, 32(4): 358~361.
- Bayliss P, Levinson A A. 1971. Low temperature hydrothermal synthesis from dolomite or calcite, quartz and kaolinite. Clays and Clay Minerals, 19: 109~114.
- Boulvais P, de Parseval P, D' Hulst A, Paris P. 2006. Carbonate alteration associated with talc—chlorite mineralization in the eastern Pyrenees, with emphasis on the St. Barthelemy Massif. Mineralogy and Petrology, 88: 499~526.
- Cai Chunfang, Zhao Long. 2016. Thermochemical sulfate reduction and its effects on petroleum composition and reservoir quality: advances and problems. Bulletin of Mineralogy, Petrology and Geochemistry, 35(5): 851~859.
- Chen Congxi, Ni Pei, Cai Keqin, Zhai Yusheng, Deng Jun. 2003. The minerogenic fluids of magnesite and talc deposits in the Paleoproterozoic Mg-rich carbonate formations in eastern Liaoning province. Geological Review, 49(6): 646~651.
- Chen C T A, Marshall W L. 1982. Amorphous silica solubilities IV. Behavior in pure water and aqueous sodium chloride, sodium sulfate, magnesium chloride, and magnesium sulfate solutions up to 350 °C. Geochimica et Cosmochimica Acta, 46(2): 279~287.
- Chen Yong. 2015#. Raman spectroscopy for fluid inclusion analysis and applications. Dongying: China University of Petroleum Press; 20~23.
- Chen Yongdi. 2012. The thermal decomposition behavior of dolomite and application. Supervisor: Cao Zhanyi. Changchun: Master Thesis of Jilin University; 1~55.
- Chou I-M, Burruss R C, Lu W J. 2005. A new optical cell for spectroscopic studies of geologic fluids at pressures up to 100 MPa. In: J. Chen, Y. Wang, T. S. Duffy, G. Shen and L. F. Dobrzinetakaya (eds.). Advances in High-Pressure Technology for Geophysical Applications. Amsterdam; Elsevier; 475~485.
- Chou I-M, Song Y, Burruss R C. 2008. A new method for synthesizing fluid inclusions in fused silica capillaries containing organic and inorganic material. Geochim. Cosmochim. Acta, 72: 5217~5231.
- Dargent M, Dubessy J, Truche L, Bazarkina EF, Nguyen-Trung C, Robert P. 2013. Experimental study of uranyl (VI) chloride complex formation in acidic LiCl aqueous solutions under hydrothermal conditions (T = 21 °C ~ 350 °C, Psat) using Raman spectroscopy. European Journal of Mineralogy, 25(5): 765~775.
- Davies G R, Smith Jr L B. 2006. Structurally controlled hydrothermal dolomite reservoir facies: An overview. AAPG Bulletin, 90(11): 1641~1690.
- Dong Shaofeng, Chen Daizhao, Qing Hairuo, Zhou Xiqiang, Wang Dan, Guo Zenghui, Jiang Maosheng, Qian Yixiong. 2013. Hydrothermal alteration of dolostones in the Lower Ordovician, Tarim Basin, NW China: Multiple constraint from petrology, isotope geochemistry and fluid inclusion microthermometry. Marine and Petroleum Geology, 46: 270~286.
- Duan Zhenhao and Li Dedong. 2008. Coupled phase and aqueous species equilibrium of the H₂O—CO₂—NaCl—CaCO₃ system from 0 to 250 °C, 1 to 1000 bar with NaCl concentrations up to saturation of halite. Geochimica et Cosmochimica Acta, 72(20): 5128~5145.
- Dubessy J, Moissette A, Bakker R J, Frantz J D, Zhang Y G. 1999. High-temperature Raman spectroscopic study of H₂O—CO₂—CH₄ mixtures in synthetic fluid inclusions: first insights on molecular interactions and analytical implications. Eur. J. Mineral., 11: 23~32.
- Eggert R G, Kerrick D M. 1981. Metamorphic equilibria in the siliceous dolomite system; 6 kbar experimental data and geologic implications. Geochimica et Cosmochimica Acta, 45: 1039~1049.
- Fall A, Tattitch B, Bodnar R J. 2011. Combined microthermometric and Raman spectroscopic technique to determine the salinity of H₂O—CO₂—NaCl fluid inclusions based on clathrate melting. Geochim. Cosmochim. Acta 75: 951~964.
- Feng Mingyou, Wu Pengcheng, Qiang Zitong, Liu Xiaohong, Duan Yong, Xia Maolong. 2017. Hydrothermal dolomite reservoir in the Precambrian Dengying Formation of central Sichuan Basin, Southwestern China. Marine and Petroleum Geology, 82: 206~219.
- Fleming B A, Crerar D A. 1982. Silicic acid ionization and calculation of silica solubility at elevated temperature and pH application to geothermal fluid processing and reinjection. Geothermics, 11(1), 15~29.
- Frezza M L, Tecce F, Casagli A. 2012. Raman spectroscopy for fluid inclusion analysis. Journal of Geochemical Exploration, 112: 1~20.
- Garrabos Y, Tufeu R, Le Neindre B, Zalczer G, Beysens D. 1980. Rayleigh and Raman scattering near the critical point of carbon dioxide. The Journal of Chemical Physics, 72: 4637~4651.
- Giles M R, Marshall J D. 1986. Constraints on the development of secondary porosity in the subsurface: re-evaluation of processes. Marine and Petroleum Geology, 3: 243~255.
- Gordon T M, Greenwood H J. 1970. The reaction dolomite + quartz + water = talc + calcite + carbon dioxide. American Journal of Science, 268: 225~242.
- Gunasekaran S, Anbalagan G, Pandi S. 2006. Raman and infrared spectra of carbonates of calcite structure. Journal of Raman Spectroscopy, 37: 892~899.
- Gunnarsson I, Arnórsson S. 2000. Amorphous silica solubility and the thermodynamic properties of H₄SiO₄ in the range of 0 to 350 °C at Psat. Geochimica et Cosmochimica Acta, 64(13): 2295~2307.
- Hao Fang, Zhang Xuefeng, Wang Cunwu, Li Pingping, Guo Tonglou, Zou Huayao, Zhu Yangming, Liu Jianzhang, Cai Zhongxian. 2015. The fate of CO₂ derived from thermochemical sulfate reduction (TSR) and effect of TSR on carbonate porosity and permeability, Sichuan Basin, China. Earth-Science Reviews, 141: 154~177.
- Hecht L, Freiburger R, Gilg H A, Grundmann G, Kostitsyn Y A. 1999. Rare earth element and isotope (C, O, Sr) characteristics of hydrothermal carbonates; genetic implications for dolomite-hosted talc mineralization at Göpfersgrün (Fichtelgebirge, Germany). Chemical Geology, 155: 115~130.
- Holness M B. 1997. Fluid flow paths and mechanisms of fluid infiltration in carbonates during contact metamorphism: the Beinn an Dubhaich aureole, Skye. Journal of Metamorphic Geology, 15: 59~70.
- Huang Sijing, Lan Yefang, Huang Keke, Lv Jie. 2014. Vug fillings and records of hydrothermal activity in the Middle Permian Qixia Formation, western Sichuan Basin. Acta Petrologica Sinica, 30(3): 687~698.

- Jiang Xiaoguang, Wang Ling, Chu Gang, Hu Xiaojing, Li Weigang, Liu Mingyang, Wang Yanjun, Lin Zhong, Sheng Xiangjun, Chen Yu. 2012&. Phase composition analysis of calcined dolomite by X-ray diffraction. *Chinese Journal of Inorganic Analytical Chemistry*, 2 (1): 31 ~ 33.
- Jiao Cunli, He Zhiliang, Xing Xiujian, Qing Hairuo, He Bizhu, Li Chengcheng. 2011&. Tectonic hydrothermal dolomite and its significance of reservoirs in Tarim basin. *Acta Petrologica Sinica*, 27 (1): 277 ~ 284.
- Jin Zhijun, Zhu Dongya, Hu Wenxuan, Zhang Xuefeng, Wang Yi, Yan Xiangbin. 2006&. Geological and geochemical signatures of hydrothermal activity and their influence on carbonate reservoir beds in the Tarim Basin. *Acta Geologica Sinica*, 80(2): 245 ~ 253.
- Lamadrid H M. 2016. Geochemistry of fluid—rock processes. Supervisor: Robert J. Bodnar. Blacksburg, VA: Virginia Polytechnic Institute and State University/Doctoral Dissertation; 1 ~ 175.
- Lan Yefang, Huang Sijing, Ma Yongkun, Zhou Xiaokang, Wei Zhe. 2016&. Genesis of negative carbon and oxygen isotopic composition of carbonate rocks in lower Miocene Zhujiang Formation, Pearl River Mouth Basin. *Geological Review*, 62(4): 915 ~ 928.
- Li Mingde. 1991&. Thermodynamic investigation of the serpentinization and talcization of the dolomite. *Mineralogy and Petrology*, 11(4): 100 ~ 104.
- Li Yingtao, Ye Ning, Yuan Xiaoyu, Huang Qingyu, Su Bingrui, Zhou Ruiqi. 2015&. Geological and geochemical characteristics of silicified hydrothermal fluids in Well Shunnan 4, Tarim Basin. *Oil & Gas Geology*, 36(6): 934 ~ 944.
- Lin Chuanxian, Bai Zhenghua, Zhang Zheru. 1985#. Handbook of thermodynamic data for minerals and related chemical compounds. Beijing: Science Press; 13 ~ 30.
- Liu Hong, Ma Teng, Tan Xiucheng, Zeng Wei, Hu Guang, Xiao Di, Luo Bing, Shan Shujiao, Su Chengpeng. 2016. Origin of structurally controlled hydrothermal dolomite in epigenetic karst system during shallow burial: An example from Middle Permian Maokou Formation, central Sichuan Basin, SW China. *Petroleum Exploration and Development*, 43: 1000 ~ 1012.
- Liu Shugen, Huang Wenming, Chen Cuihua, Zhang Changjun, Li Juchu, Dai Sulan, Qin Chuan. 2008&. Primary study on hydrothermal fluids activities and their effectiveness on petroleum and mineral accumulation of Sinian—Palaeozoic in Sichuan Basin. *J. Mineral. Petrol.*, 28(3): 41 ~ 50.
- Liu Shugen, Ma Yongsheng, Huang Wenming, Cai Xunyu, Zhang Changjun, Wang Guozhi, Pan Changlin. 2007&. Densification process of Upper Sinian Dengying Formation, Sichuan Basin. *Natural Gas Geoscience*, 18(4): 485 ~ 496.
- Liu Yingchao, Song Yucai, Hou Zengqian, Yang Zhusen, Zhang Hongrui, Ma Wang. 2015. The Malyer—Esfahan carbonate-hosted Pb—Zn metallogenic belt in the Zagros collisional orogen of Iran: Characteristics and genetic types. *Acta Geologica Sinica*, 89(9): 1573 ~ 1594.
- Lonnee J, Machel H G. 2006. Pervasive dolomitization with subsequent hydrothermal alteration in the Clarke Lake gas field, Middle Devonian Slave Point Formation, British Columbia, Canada. *AAPG Bulletin*, 90: 1739 ~ 1761.
- Lu Wanjun, Guo Huirong, Chou I-M, Burruss R C, Li L. 2013. Determination of diffusion coefficients of carbon dioxide in water between 268 and 473 K in a high-pressure capillary optical cell with in situ Raman spectroscopic measurements. *Geochimica et Cosmochimica Acta*, 115: 183 ~ 204.
- Lu Wanjun, Chou I-M, Burruss R C, Song Yucai. 2007. A unified equation for calculating methane vapor pressures in the CH₄—H₂O system with measured Raman shifts. *Geochim. Cosmochim. Acta*, 71: 3969 ~ 3978.
- Luczaj J A, Harrison III W B, Williams N S. 2006. Fractured hydrothermal dolomite reservoirs in the Devonian Dundee Formation of the central Michigan Basin. *AAPG Bulletin*, 90(11): 1787 ~ 1801.
- Luczaj J A. 2006. Evidence against the Dorag (mixing-zone) model for dolomitization along the Wisconsin arch — A case for hydrothermal diagenesis. *AAPG Bulletin*, 90: 1719 ~ 1738.
- Machel H G. 2004. Concepts and models of dolomitization: a critical reappraisal. In: Braithwaite, C. J. R., Rizzi, G., Darke, G. (Eds.). *The Geometry and Petrogenesis of Dolomite Hydrocarbon Reservoirs*. Geological Society of London, Special Publication, 235: 7 ~ 63.
- Machel H G, Lonnee J. 2002. Hydrothermal dolomite—a product of poor definition and imagination. *Sedimentary Geology*, 152: 163 ~ 171.
- Marshall W. 1980. Amorphous silica solubilities—I. Behavior in aqueous sodium nitrate solutions; 25 ~ 300 °C, 0 ~ 6 molal. *Geochimica et Cosmochimica Acta*, 44(7): 907 ~ 913.
- McKinley J M, Worden R H, Ruffell A H. 2001. Contact diagenesis: the effect of an intrusion on reservoir quality in the Triassic Sherwood Sandstone Group, Northern Ireland. *Journal of Sedimentary Research*, 71: 484 ~ 495.
- Nicola J H, Scott J F, Couto R M, Correa M M. 1976. Raman spectra of dolomite [CaMg(CO₃)₂]. *Physical Review B*, 14: 4676.
- Packard J J, Al-Aasm I, Samson I, Berger Z, Davies J. 2001. A Devonian hydrothermal chert reservoir: the 225 bcf Parkland field, British Columbia, Canada. *AAPG Bulletin*, 85(1): 51 ~ 84.
- Pan Wenqing, Liu Yongfu, Dickson JAD, Shen Anjiang, Han Jie, Ye Ying, Gao Hongliang, Guan Ping, Zhang Lijuan, Zheng Xingping. 2009&. The Geological model of hydrothermal activity in outcrop and the characteristics of carbonate hydrothermal karst of Lower Paleozoic in Tarim Basin. *Acta Sedimentologica Sinica*, 27(5): 983 ~ 994.
- Pan Zhiyan, Chou I-M, Burruss R C. 2009. Hydrolysis of polycarbonate in sub-critical water in fused silica capillary reactor with in situ Raman spectroscopy. *Green Chemistry*, 11(8): 1105 ~ 1107.
- Parker Jr J H, Feldman D W, Ashkin M. 1967. Raman scattering by silicon and germanium. *Phys. Rev.*, 155: 712 ~ 714.
- Pokrovsky O S, Golubev S V, Schott J. 2005. Dissolution kinetics of calcite, dolomite and magnesite at 25 °C and 0 to 50 atm pCO₂. *Chemical Geology*, 217: 239 ~ 255.
- Pokrovsky O S, Golubev S V, Schott J, Castillo A. 2009. Calcite, dolomite and magnesite dissolution kinetics in aqueous solutions at acid to circumneutral pH, 25 to 150°C and 1 to 55 atm pCO₂: New constraints on CO₂ sequestration in sedimentary basins. *Chemical Geology*, 265: 20 ~ 32.
- Povoden E, Horacek M, Abart R. 2002. Contact metamorphism of siliceous dolomite and impure limestones from the Werfen formation in the eastern Monzoni contact aureole. *Mineralogy and Petrology*, 76: 99 ~ 120.
- Qi Lixin. 2016&. Oil and gas breakthrough in ultra-deep Ordovician carbonate formations in Shuntuoguole uplift, Tarim Basin. *China Petroleum Exploration*, 21(3): 38 ~ 51.
- Qing Hairuo, Mountjoy E W. 1994. Formation of coarsely crystalline, hydrothermal dolomite reservoirs in the Presqu'ile Barrier, Western Canada sedimentary basin. *AAPG Bulletin* 78(1): 55 ~ 77.
- Qing Hairuo. 2017. An introduction of petrology and diagenesis of ultra-deep water carbonate reservoirs from the Atlantic Ocean, offshore

- Brazil. Oral presentation at Wuxi Institute of Petroleum Geology of SINOPEC, Wuxi, China.
- Rosasco G J, Blaha J J. 1980. Raman microprobe spectra and vibrational mode assignments of talc. *Applied Spectroscopy*, 34: 140 ~ 144.
- Rosso K M, Bodnar R J. 1995. Microthermometric and Raman spectroscopic detection limits of CO₂ in fluid inclusions and the Raman spectroscopic characterization of CO₂. *Geochim. Cosmochim. Acta*, 59: 3961 ~ 3975.
- Seewald J S. 2003. Organic—inoorganic interactions in petroleum-producing sedimentary basins. *Nature*, 426: 327 ~ 333.
- Shang Linbo, Chou I-M, Lu W, Burruss R C, Zhang Y. 2009. Determination of diffusion coefficients of hydrogen in fused silica between 296 and 523 K by Raman spectroscopy and application of fused silica capillaries in studying redox reactions. *Geochimica et Cosmochimica Acta*, 73(18): 5435 ~ 5443.
- Sharma R, Joshi P, Pant P D. 2009. The role of fluids in the formation of talc deposits of Rema area, Kumaun Lesser Himalaya. *Journal of the Geological Society of India*, 73: 237 ~ 248.
- Shock E L, Helgeson H C. 1988. Calculation of the thermodynamic and transport properties of aqueous species at high pressures and temperatures: Correlation algorithms for ionic species and equation of state predictions to 5 kb and 1000°C. *Geochimica et Cosmochimica Acta*, 52: 2009 ~ 2036.
- Shu Xiaohui, Zhang Juntao, Li Guorong, Long Shengxiang, Wu Shixiang, Li Hongtao. 2012. Characteristics and genesis of hydrothermal dolomites of Qixia and Maokou formations in northern Sichuan Basin. *Oil & Gas Geology*, 33(3): 443 ~ 448, 458.
- Skippen G. 1974. An experimental model for low pressure metamorphism of siliceous dolomitic marble. *American Journal of Science*, 274: 487 ~ 509.
- Slater B E, Smith Jr L B. 2012. Outcrop analog for Trenton-Black River hydrothermal dolomite reservoirs, Mohawk Valley, New York. *AAPG Bulletin*, 96(7): 1369 ~ 1388.
- Slaughter J, Kerrick D M, Wall V J. 1975. Experimental and thermodynamic study of equilibria in the system CaO—MgO—SiO₂—H₂O—CO₂. *American Journal of Science*, 275: 143 ~ 162.
- Smith L B Jr. 2006. Origin and reservoir characteristics of Upper Ordovician Trenton-Black River hydrothermal dolomite reservoirs in New York. *AAPG Bulletin*, 90: 1691 ~ 1718.
- Song Yucai, Chou I-M, Hu W, Burruss R C, Lu W. 2009. CO₂ density-Raman shift relation derived from synthetic inclusions in fused silica capillaries and its application. *Acta Geol. Sin.* 83: 932 ~ 938.
- Tang Xuesong, Tan Xiucheng, Liu Hong, Ma Teng, Su Chengpeng, Cheng Xueying, Chen Hongyu, Cao Jian. 2016. Characteristics and development mechanism of dolomite and dolomitic quartzite reservoirs of the Middle Permian Maokou Formation in eastern Sichuan Basin. *Oil and Gas Geology*, 37(5): 731 ~ 743.
- Tornos F, Spiro B F. 2000. The geology and isotope geochemistry of the talc deposits of Puebla de Lillo (Cantabrian Zone, Northern Spain). *Economic Geology*, 95: 1277 ~ 1296.
- Wan Ye, Wang Xiaolin, Chou I-M, Hu Wenxuan. 2017. An experimental study of the formation of talc through CaMg(CO₃)₂—SiO₂—H₂O interaction at 100 ~ 200°C and vapor-saturation pressures. *Geofluids*, 2017: 3942826, 1 ~ 14.
- Wan Ye, Wang Xiaolin, Hu Wenxuan, Chou I-M. 2015. Raman spectroscopic observations of the ion association between Mg²⁺ and SO₄²⁻ in MgSO₄-saturated droplets at temperatures of ≤ 380°C. *The Journal of Physical Chemistry A*, 119(34): 9027 ~ 9036.
- Wang Xiaolin, Chou I-M, Hu Wenxuan, Burruss R C. 2013a. In situ observations of liquid—liquid phase separation in aqueous MgSO₄ solutions: geological and geochemical implications. *Geochimica et Cosmochimica Acta*, 103: 1 ~ 10.
- Wang Xiaolin, Chou I-Ming, Hu Wenxuan, Yuan Shunda, Liu Hao, Wan Ye, Wang Xiaoyu. 2016c. Kinetic inhibition of dolomite precipitation: Insights from Raman spectroscopy of Mg²⁺—SO₄²⁻ ion pairing in MgSO₄/MgCl₂/NaCl solutions at temperatures of 25 to 200°C. *Chemical Geology*, 435: 10 ~ 21.
- Wang Xiaolin, Hu Wenxuan, Chou I-Ming. 2013b. Raman spectroscopic characterization of the OH stretching bands in NaCl—Na₂CO₃—Na₂SO₄—CO₂—H₂O systems: Implications for the measurement of chloride concentrations in fluid inclusions. *J. Geochem. Explor.*, 132: 111 ~ 119.
- Wang Xiaolin, Hu Wenxuan, Yao Suping, Chen Qi, Xie Xiaomin. 2011a. Carbon and strontium isotopes and global correlation of Cambrian Series 2—Series 3 carbonate rocks in the Keping area of the northwestern Tarim Basin, NW China. *Marine and Petroleum Geology*, 28: 992 ~ 1002.
- Wang Xiaolin, Wan Ye, Hu Wenxuan, Chou I-Ming, Cai Shenyang, Lin Nan, Zhu Qiang, Li Zhen. 2016b. Visual and in situ Raman spectroscopic observations of the liquid—liquid immiscibility in aqueous uranyl sulfate solutions at temperatures up to 420°C. *The Journal of Supercritical Fluids*, 112: 95 ~ 102.
- Wang Xiaolin, Wan Ye, Hu Wenxuan, Chou I-Ming, Cao Jian, Wang Xiaolin, Wang Meng, Li Zhen. 2016a. In situ observations of liquid—liquid phase separation in aqueous ZnSO₄ solutions at temperatures up to 400°C: Implications for Zn²⁺—SO₄²⁻ association and evolution of submarine hydrothermal fluids. *Geochimica et Cosmochimica Acta*, 181: 126 ~ 143.
- Wang Xiaolin, Wang Xiaoyu, Chou I-Ming, Hu Wenxuan, Wan Ye, Li Zhen. 2017. Properties of lithium under hydrothermal conditions revealed by in situ Raman spectroscopic characterization of Li₂O—SO₃—H₂O(D₂O) systems at temperatures up to 420°C. *Chemical Geology*, 451: 104 ~ 115.
- Wang Xiaolin, Chou I-M, Hu W, Burruss R C, Sun Q, Song Y. 2011b. Raman spectroscopic measurements of CO₂ density: Experimental calibration with high-pressure optical cell (HPOC) and fused silica capillary capsule (FSCC) with application to fluid inclusion observations. *Geochimica et Cosmochimica Acta*, 75: 4080 ~ 4093.
- Warren J. 2000. Dolomite; occurrence, evolution and economically important associations. *Earth-Science Reviews*, 52(1 ~ 3): 1 ~ 81.
- White D. E. 1957. Thermal waters of volcanic origin. *Geological Society of America Bulletin*, 68, 1637 ~ 1658.
- Wright R B, Wang C H. 1973. Density effect on the Fermi resonance in gaseous CO₂ by Raman scattering. *The Journal of Chemical Physics*, 58: 2893.
- Yamamoto J, Kagi H. 2006. Extended micro-Raman densimeter for CO₂ applicable to mantle-originated fluid inclusions. *Chem. Lett.* 35, 610 ~ 611.
- Yuan Shunda, Chou I-M, Burruss R C, Wang X. 2013. Disproportionation and thermochemical sulfate reduction reactions in S—H₂O—CH₄ and S—D₂O—CH₄ systems from 200 to 340 °C at elevated pressures. *Geochimica et Cosmochimica Acta*, 118: 263 ~ 275.
- Yun Lu, Cao Zicheng. 2014. Hydrocarbon enrichment pattern and exploration potential of the Ordovician in Shunnan area, Tarim Basin. *Oil and Gas Geology*, 35(6): 788 ~ 797.
- Zhu Dongya, Hu Wenxuan, Song Yucai, Jin Zhijun. 2005. Fluoritization in Tazhong 45 reservoir: characteristics and its effect

on the reservoir bed. *Acta Petrologica et Mineralogica*, 24(3): 205 ~ 215.

Zhu Dongya, Jin Zhijun, Hu Wenxuan, Zhang Xuefeng. 2008&. Effects of deep fluid on carbonates reservoir in Tarim basin. *Geological Review*, 54(3): 348 ~ 354.

Zhu Dongya, Jin Zhijun, Hu Wenxuan. 2009&. Hydrothermal alteration dolomite reservoir in Tazhong area. *Acta Petrolei Sinica*, 30(5): 698 ~ 704.

Zhu Dongya, Meng Qingqiang, Jin Zhijun, Hu Wenxuan. 2015b. Fluid

environment for preservation of pore spaces in a deep dolomite reservoir. *Geofluids*, 15: 527 ~ 545.

Zhu Dongya, Meng Qingqiang, Jin Zhijun, Liu Quanyou, Hu Wenxuan. 2015a. Formation mechanism of deep Cambrian dolomite reservoirs in the Tarim basin, northwestern China. *Marine and Petroleum Geology*, 59: 232 ~ 244.

Zhu Dongya, Meng Qingqiang. 2010&. The genesis of silicification in the Lower Paleozoic carbonate in the Tarim Basin. *Petroleum Geology & Experiment*, 32(4): 358 ~ 361.

Experimental Studies on the Interactions between Dolomite and SiO₂-rich Fluids: Implications for the Formation of Carbonate Reservoirs

WANG Xiaolin^{1,2)}*, WAN Ye¹⁾, HU Wenxuan^{1,2)}, YOU Donghua³⁾, CAO Jian^{1,2)},
ZHU Dongya⁴⁾, LI Zhen⁵⁾

1) School of Earth Sciences and Engineering, Nanjing University, Nanjing, 210023, China;

2) Institute of Energy Sciences, Nanjing University, Nanjing, 210023, China;

3) Research Institute of Experimental Geology, SINOPEC Petroleum Exploration and Production Research Institute, Wuxi, Jiangsu, 214151, China;

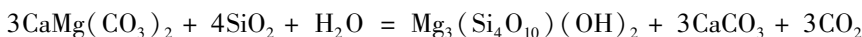
4) Petroleum Exploration and Production Research Institute of SINOPEC, Beijing, 100083, China;

5) The Institute for Geoscience Research, Department of Applied Geology, Curtin University, GPO Box U1987, Perth, WA 6485, Australia

Objectives: Investigating the water—rock interaction mechanism and kinetics between dolomite and silica-rich hydrothermal fluids; Discussing the effect of silica-rich hydrothermal fluids on the formation of deep carbonate hydrocarbon reservoirs.

Methods: Fused silica capillary tubes were used as reaction cells. Dolomite/calcite powder and deionized water were loaded into the fused silica capillary tube, which was made from pure silica. Thus, the silica involved in the water—rock interaction was from the dissolution of the tube; The vapor phase was in situ measured using a high resolution Raman spectroscopy (LabRAM HR800) with a spectral resolution of $\sim 1 \text{ cm}^{-1}$. The quenched solid products were analyzed using Raman spectroscopy, micro-X-ray diffraction (D/max Rapid II, Rigaku), field emission scanning electron microscope (Supra55, Zeiss) equipped with an energy dispersive spectrometer (Oxford Instruments, Inca X-Max 150 mm²).

Results: Dolomite can react with Si-rich fluid to form talc, calcite and CO₂ at temperatures above 100°C. The reaction can be described as:



The reaction was promoted by high temperature and/or lower partial pressure of CO₂. In other words, high temperature and the presence of a conduit to release CO₂ will promote the formation of talc; Talc and other Mg-rich silicate minerals can be used to trace the activity of silica-rich hydrothermal fluids in dolomite sequences. If silica originated from quartz/chert within the dolomite sequence, the hydrothermal alteration of dolomite by silica-rich fluids would increase the porosity of dolomite reservoirs; In the Shuotuoquole area of Tarim Basin, silica-rich hydrothermal fluids migrated upwards to the Yingshan Formation through deep faults. The interaction between the silica-rich fluids and the Sinian—Cambrian dolomite would result in the formation of talc and CO₂. Then, the produced CO₂ ascends to the shallow limestone sequence of Yingshan Formation and promoted the dissolution of limestone to form large amounts of pores. The precipitation of micro-quartz in the Yingshan Formation was favored by (a) decreasing temperature due to mixing between hydrothermal fluids and formation water, and (b) the presence of CO₂. The results also support the view that the silica-rich hydrothermal fluids responsible for the precipitation of micro-quartz in the Shuntuoquole area were depleted in Mg.

Keywords: dolomite; SiO₂-rich fluid; water—rock interaction; talc; carbonate reservoir

Acknowledgements: This work was financially supported by the National Natural Science Foundation of China

(Grant nos. 41573054 and 41230312) and the Fundamental Research Funds for the Central Universities (020614380056). We thank Prof. Xiucheng Tan of Southwest Petroleum University for providing geological evidences supporting the formation of talc through dolomite—silica—water interaction. The manuscript benefits a lot from the constructive comments from the editor and two anonymous reviewers.

First author: WANG Xiaolin, male, born in 1982, associate professor in high P — T experimental geochemistry and carbonate reservoir geology. Email: xlinwang@nju.edu.cn.

Manuscript received on:2017-07-03;Accepted on:2017-11-01;Edited by:LIU Zhiqiang

Doi: 10.16509/j. georeview. 2017. 06. 017

(上接第 1478 页)

大会特邀张培震, 杨树锋, 赵文智等三位院士、朱立新, 李子颖, 王京彬, 侯增谦, 张招崇、王登红、熊盛青、殷跃平、林君、彭云彪等十位研究员、教授或教授级高工在主场作了主题报告。他们的报告题目依次是: 青藏高原现今构造变形与深部动力作用、塔里木大火成岩省的研究、如何看待中国的油气资源潜力与未来发展前景、深部及覆盖区地球化学勘查新进展、中国砂岩铀矿成矿理论创新与找矿重大突破、综合地质调查——思考与探索、特提斯构造域碰撞造山与成矿、岩浆—热液演化与块状磁铁矿石的成因、锂矿床找矿进展与发展趋势、航空地球物理与深地资源勘查、高速远程灾害滑坡研究及防灾对策、深地资源探测仪器自主研发与应用、内蒙古中西部砂岩型铀矿勘查实践。中国地质学会常务副理事长孟宪来主持了大会主题报告。

袁道先院士、裴荣富院士等在分组会上作了学术报告。

12日进行了野外地质考察, 有长兴—安吉野外地质考察和诸暨璜山—陈蔡地区野外地质考察两条线路。长兴—安吉线考察内容为: 煤山全球二叠系—三叠系界线层型剖面 and 煤山长兴阶标准层型剖面, 下扬子区安吉赫南特阶标准剖面, 并顺路参观了“绿水青山就是金山银山”理论发源

地——安吉余村。诸暨线考察内容为: 璜山杂岩体石角超镁铁质球状岩、璜山杂岩体青顶山新元古代洋内弧岩浆岩岩石组合、陈蔡俯冲增生杂岩洋岛—海山岩石组合, 顺道参观了东白湖镇斯宅清代古民居——千柱屋。浙江省地质调查院为野外地质考查提供了全方位的帮助和鼎力支持, 9月份即进行前期路线的拟定、规划和安排, 会议前多次野外实地路线踏勘, 考察当天派出10位讲解员和2辆考察引导车。

浙江省地质学会及浙江省地质勘查局、浙江省第一地质大队、浙江省第七地质大队、中化地质矿山总局浙江地质勘查院、中国建筑材料工业地质勘查中心浙江总队等, 在学会副理事长兼秘书长倪悦亲自带领下, 为此次会议的顺利召开作出了重要贡献。

Promoting Innovation of Geological Science and Technology, to Help Green Economic Development: the 2017's Conference of the Geological Society of China Held in Hangzhou

(据 <http://www.geosociety.org.cn/?category=bmV3cw==&catiegodry=NzEzNg==>, 有增删)

